FINITE ELEMENT COMPUTATION OF VISCOUS FLOWS IN SUPERSONIC WIND-TUNNEL

S. Mittal, S. Yadav, S. Bajaj, V. Gupta
Department of Aerospace Engineering, IIT, Kanpur.

ABSTRACT

A stabilized finite element formulation for the computation of viscous, unsteady flows in supersonic wind-tunnels is developed and implemented. The governing equations are the unsteady Navier-Stokes equations in the conservation law form. The implementation is based on the implicit formulation of the governing equations and non-linear boundary conditions and conservation variables are employed. The equation systems, resulting from the discretization, are solved iteratively by using the preconditioned GMRES technique. Results are presented for flow through a tunnel with a Mach 5 minimum-length nozzle for various diffuser geometries. For a particular diffuser geometry, the effect of the reservoir to exit pressure-ratio is investigated. In one of the simulations the start-up problem of the wind-tunnel with a diffuser of small cross-section area is investigated.

INTRODUCTION

Stabilised finite-element formulations are employed to compute viscous flows in supersonic wind tunnels. The Navier-Stokes equations are cast in their conservation law form and the finite element method based on the conservation variables formulation is utilised to solve the flow equations on unstructured meshes with triangular elements. The solution to the equation system from the finite element discertization is computed via the GMRES (Generalized Minimal RESidual) method in conjunction with block-diagonal preconditioners. The tunnel consists of a nozzle block, test section and diffuser. A typical geometry is shown in Figure 1.

The converging-diverging minimum-length nozzle is designed by the method of characteristics for Mach 5 inviscid flow. The test-section to nozzle throat area ratio is 25. The half-height of the test-section is A_1 and the length is $2A_1$. The various parameters in the diffuser geometry that influence its performance are A_2/A_1 , Lc, Ls, and the convergent and divergent angles. In the present study, the angles of the diffuser are fixed to 10 deg. and the effect of all other parameters in the diffuser geometry is studied. In one of the cases that is considered the area ratio A_2/A_1 is much smaller than the critical value below, which the tunnel fails to start. The effect of the exit-to-reservoir pressure ratio is also investigated. The present work is expected to lead to a better understanding of the supersonic diffuser and to a powerful tool for design of supersonic diffusers.

The finite element formulations employed in this work are well proven and have been applied on many problems involving external flows. For example, see the articles by Mittal [1,2]. The formulations are being extended to the study of internal flows. They have been tested on standard benchmark problems (for example, supersonic flow through a duct with two throats presented in a GAMM workshop) and produced satisfactory results. There have been several computational efforts in the past by various other researchers relating to various components in this study. Polsky and Cambier [3] studied the transient flow through a shock tunnel using Euler equations, Chen, Chakravarthy and Hung [4] used the Reynolds-averaged Navier-Stokes equations to study separated flow through converging-diverging nozzles and Agrow and Emanuel [5] investigated transonic flow field in a 2D minimum length nozzle.

THE GOVERNING EQUATIONS

Let $\Omega \subset \Re^{n_{sd}}$ and (0,T) be spatial and temporal domains respectively, where n_{sd} is the number of space dimensions, and let Γdenote the boundary of Ω. The spatial and temporal co-ordinates are denoted by x and t. The Navier-Stokes equations governing the fluid flow, in conservation form, are

$$\frac{\partial \rho}{\partial t} + \nabla.(\rho u) = 0 \qquad \text{on } \Omega \text{ for } (0,T)$$

$$\frac{\partial (\rho u)}{\partial t} + \nabla.(\rho u u) + \nabla p - \nabla.T = 0 \qquad \text{on } \Omega \text{ for } (0,T) \qquad \ldots(2)$$

$$\frac{\partial (\rho e)}{\partial t} + \nabla.(\rho e u) + \nabla.(pu) - \nabla.(Tu) + \nabla q = 0 \qquad \text{on } \Omega \text{ for } (0,T) \qquad \ldots(3)$$

Here ρ, u, p, T, e and q are the density, velocity, pressure, viscous stress tensor, the total energy per unit mass, and the heat flux vector, respectively. The viscous stress tensor is defined as

$$T = \mu\left((\nabla u) + (\nabla u)^T\right) + \lambda(\nabla.u)I. \qquad \ldots(4)$$

Where μ and λ are the viscosity coefficients. It is assumed that μ and λ are related by

$$\lambda = -\frac{2}{3}\mu \qquad \ldots(5)$$

Pressure is related to the other variables via the equation o state. For ideal gases, the equation of state assumes th special form

$$p = (\gamma - 1)\rho i \quad \ldots(6)$$

where γ is the ratio of specific heats and i is the interna energy per unit mass that is related to the total energy pe unit mass and velocity as

$$i = e - \frac{1}{2}\|u\|^2 \quad \ldots(7)$$

The heat flux vector is defined as

$$q = -k\nabla\theta \quad \ldots(8)$$

where k is the heat conductivity and θ is the temperature The temperature is related to the internal energy by th following relation

$$\theta = \frac{\gamma - 1}{R} i \quad \ldots(9)$$

where R is the ideal gas constant. Prandtl number (Pr) assumed to be specified, relates the heat conductivity to th fluid viscosity according to the following relation

$$k = \frac{\gamma R \mu}{(\gamma - 1)\ \mathrm{Pr}} \quad \ldots(10)$$

The compressible Navier-Stokes equations (1), (2), and (3) can be written in the conservation variables

$$\frac{\partial U}{\partial t} + \frac{\partial \mathrm{F}_i}{\partial \mathrm{x}_i} - \frac{\partial \mathrm{E}_i}{\partial \mathrm{x}_i} = 0 \qquad \text{on } \Omega \text{ for } (0,\mathrm{T}) \quad \ldots(11)$$

where $= (\rho, \rho u_1, \rho u_2, \rho \mathrm{e})$, is the vector of conservation variables, and F_i and E_i are, respectively the Euler and viscous flux vectors defined as

$$F_i = \begin{pmatrix} u_i\,\rho \\ u_i\,\rho\,u_1 + \delta_{i1}p \\ u_i\,\rho\,u_2 + \delta_{i2}p \\ u_i\,(\rho\,\mathrm{e} + p) \end{pmatrix} \quad \ldots(12)$$

$$E_i = \begin{pmatrix} 0 \\ \tau_{i1} \\ \tau_{i2} \\ -q_i + \tau_{ik}u_k \end{pmatrix} \quad \ldots(13)$$

Here u_i, q_i *and* τ_{ik} are the components of the velocity, heat flux, and viscous stress tensor, respectively. In the quasi-linear form, equation (11) is written as

$$\frac{\partial U}{\partial t} + A_i \frac{\partial \mathrm{U}}{\partial \mathrm{x}_i} - \frac{\partial}{\partial \mathrm{x}_i}\left(K_{ij}\frac{\partial \mathrm{U}}{\partial \mathrm{x}_j}\right) = 0 \qquad \text{on } \Omega \text{ for } (0,\mathrm{T}) \quad \ldots(14)$$

wnere

$$A_i = \frac{\partial F_i}{\partial U}, \quad \ldots(15)$$

is the Euler Jacobian Matrix, and K_{ij} is the diffusivity matrix satisfying

$$K_{ij}\frac{\partial \mathrm{U}}{\partial \mathrm{x}_j} = E_i \quad \ldots(16)$$

Corresponding to equation (14), the following boundary and initial conditions are chosen

$$= g \qquad \text{on } \Gamma_g \text{ for } (0,\mathrm{T}) \quad \ldots(17)$$

$$n.E = h \qquad \text{on } \Gamma_h \text{ for } (0,\mathrm{T}) \quad \ldots(18)$$

$$(x,0) = U_0 \qquad \text{on } \Omega_0 \quad \ldots(19)$$

FINITE ELEMENT FORMULATION

Consider a finite element discretization of Ω in to subdomains Ω^e ,e = 1,2,..., n_{el}, where n_{el} is the number of elements. Based on this discretization, we define the finite element trial function space S^h and weighting function space v^h . These function spaces are selected, by taking the Dirichlet boundary conditions into account, as subsets of $\left[H^{1h}(\Omega)\right]^{n_{dof}}$ *where* $H^{1h}(\Omega)$ is the finite-dimensional function space over Ω and n_{dof} is the number of degrees of freedom.

$$S^h = \left\{U^h \middle| U^h \in \left[H^{1h}(\Omega)\right]^{n_{dof}}, U^h\big|_{\Omega\Gamma} \in \left[P^1(\Omega)\right]^{n_{dof}}, U^h.e_k = g_k \text{ on } \Gamma_{gk}\right. \quad \ldots(20)$$

$$v^h = \left\{W^h \middle| W^h \in \left[H^{1h}(\Omega)\right]^{n_{dof}}, W^h\big|_{\Omega\Gamma} \in \left[P^1(\Omega)\right]^{n_{dof}}, W^h.e_k = 0 \text{ on } \Gamma_{gk}\right. \quad \ldots(21)$$

where $\left[P^1(\Omega^e)\right]$ represents the first order polynomial in Ω^e, and k = 1,..., n_{dof}. The stabilized finite element formulation of Eq. (14) is written as follows: find

$$^h \in S^h \ such\ that\ \forall W^h \in v^h,$$

$$\int_\Omega W^h\left(\frac{\partial U}{\partial t} + A_i^h\frac{\partial U^h}{\partial \mathrm{x}_i}\right)d\Omega + \int_\Omega\left(\frac{\partial \mathrm{W}^h}{\partial \mathrm{x}_i}\right)\left(K_{ij}^h\frac{\partial U^h}{\partial \mathrm{x}_j}\right)d\Omega$$

$$+\sum_{e=1}^{n_{el}}\int_{\Omega\Gamma}\tau(A_k^h)^T\left(\frac{\partial \mathrm{W}^h}{\partial \mathrm{x}_k}\right)\left[\frac{\partial U^h}{\partial t} + A_i^h\frac{\partial U^h}{\partial \mathrm{x}_i} - \frac{\partial}{\partial x_i}\left(K_{ij}^h\frac{\partial U^h}{\partial \mathrm{x}_j}\right)\right]d\Omega$$

$$+\sum_{e=1}^{n_{el}}\int_{\Omega\Gamma}\delta\left(\frac{\partial \mathrm{W}^h}{\partial \mathrm{x}_i}\right)\left(\frac{\partial U^h}{\partial \mathrm{x}_i}\right)d\Omega = \int_{\Gamma_h} W^h.h^h\,d\Gamma \quad \ldots(22)$$

In the variational formulation given by Eq. (22), the first two terms and the right-hand-side constitute the Galerkin formulation of the problem. The first series of element-level integrals in Eq. (22) are the SUPG stabilization terms added to the variational formulation to stabilize the computations against node-to-node oscillations in the advection-dominated range. The second series of element level integrals in the formulation are the shock capturing terms that stabilize the computations in the presence of

sharp gradients. The stabilization coefficients δ and τ defined as

$$\tau = \max[0, \tau_a - \tau_\delta] \quad .(23)$$

$$\tau_a = \left[\left(\frac{2(c+\|u\|)}{h}\right)^2 + \left(\frac{12\nu}{h^2}\right)^2\right]^{-\frac{1}{2}} I \quad .(24)$$

$$\frac{\delta}{2(c+\|u\|)^2} I \quad (25)$$

$$\left[\left\|\frac{\partial U}{\partial t} + A_i \frac{\partial U}{\partial x_i}\right\|_{A_0^{-1}} \Big/ \left\|J_{1i}\frac{\partial U}{\partial x_i}\right\|_{A_0^{-1}} + \left\|J_{2i}\frac{\partial U}{\partial x_i}\right\|_{A_0^{-1}}\right] \quad (26)$$

where c is the wave speed, h is the element length, J_{ik} are the components of Jacobian transformation matrix from physical to the local co-ordinates and A_0^{-1} is the inverse of Reimannian metric tensor related to the transformation between the conservation and entropy variables [6]. Matrix τ_δ is subtracted from τ_a to account for the shock-capturing term as shown in Eq. (23). The time discretization of the variational formulation given by Eq. (22) is done via the generalized trapezoidal rule.

RESULTS AND DISCUSSIONS

Figure 1 shows a typical wind tunnel that is simulated in the present work. It also indicates the boundary conditions used in the computations. At the upstream boundary the stagnation pressure (p_0) and total enthalpy (h_0) are specified along with the direction of the flow (along the x-axis). The flow velocity at the inlet is unknown and so is the density. It is assumed that the flow between the reservoir and upstream boundary is isentropic and this condition is used to relate the density and pressure at the upstream boundary to the ones at reservoir (stagnation values). The walls of the tunnel are assumed to be maintained at the stagnation temperature and the velocity satisfies the no-slip condition. At the outlet, the exit pressure is specified while the viscous stress vector is assigned a zero value. In most of the calculations, to save on the computational expenses, only one half of the tunnel is simulated and symmetry conditions are imposed along the tunnel centre-line: the vertical component of the velocity is set to zero and so are the viscous and heat flux vectors. All the boundary conditions are implemented in an implicit manner that leads to their strong enforcement and minimize the associated numerical instabilities. The computations are initiated with zero flow condition and the pressure in the entire domain in initialized to a value corresponding to the exit pressure (p_e). The pressure at the inlet is ramped to its final value (= p_0) in 100 time units (non-dimensionalized with respect to the test-section half height, A_1 and the speed of sound at reservoir). Physically, this corresponds to the linear opening of the valve downstream of the pressurized gas tank for the blow-down. Typically, the time-step used in the computation is 0.1. The Reynolds number, based on the test section half-height (A_1), speed of sound, density and viscosity at reservoir conditions, is 10^7. Equal-in-order-interpolation linear elements are used for the computations. The finite-element mesh consists of a few layers of structured mesh close to the tunnel walls and the rest of the domain is filled with an unstructured mesh obtained via Delaunays's triangulation.

Figure 2 shows the finite element mesh and the mach contours at various time instants of a simulation, with A_2/A_1=0.3 and p_o/p_e=500. It is well know that with this area ratio, irrespective of the pressure ratio, the tunnel should not start. Our computations lead to the same observation. In the early stages of the simulation, as the upstream pressure builds up, the flow develops in the nozzle and appears like an overexpanded jet. The pulsating behaviour of the flow and the attraction of the jet towards the tunnel wall due to Coanda Effect can be observed from the figure. Figure 3 shows the variation of the centre-line pressure and mach number for various times.

Next, for a fixed reservoir to exit pressure ratio (p_o/p_e=25), the effect of the diffuser to test-section area ratio (A_2/A_1) is studied. Figures 4 and 5 show the time evolution of the flow through the tunnel for a diffuser with A_2/A_1=0.6. Beyond a certain time, the flow develops very slowly. The computations have been carried out for a very large non-dimensional time. Not much change is observed between t = 10,000 and t = 25,000. Therefore, it can be concluded that the tunnel fails to start with this diffuser geometry too. Figures 6 and 7 show the results of the computations for a diffuser with A_2/A_1=0.7. After the initial transience, the flow in the tunnel is established. Since the nozzle is designed for inviscid flow, it is not optimal for viscous flows and weak shocks can be observed in the nozzle block and the test section. The undulating boundary layer thickness in the constant area section of the diffuser due to the reflected oblique shock system can be noticed. The present mesh is not fine enough to resolve the interesting shock-wave/boundary-layer interaction. We are currently working on adaptive methods to resolve these flow structures in greater detail. From the variation of the steady-state pressure along the tunnel centreline it can be observed that most of the pressure recovery takes place in the constant-area section of the diffuser before the divergent section and very little contribution from the downstream part. The centre-line outflow mach number is approximately 1.1. However, the boundary layer is thick and a significant portion of the outflow close to the wall is subsonic. Results for A_2/A_1= 0.8 are shown in Figures 8 and 9. From these figures it can be concluded that the efficiency of the diffuser for this area ratio is lower than that for A_2/A_1 = 0.7. A shock in the nozzle block causes the flow to separate and consequently the core of the flow in the test section is far from being one-dimensional. From the plot for steady-state variation of pressure and mach

number at the tunnel centre-line, it can be observed that the pressure recovery in the later half of the diffuser is quite negligible. From this study it can be concluded that of all the cases studied so far, the diffuser with A_2/A_1=0.7 delivers the best results.

In the next part of the study the effect of the reservoir to exit pressure ratio is investigated for the diffuser with A_2/A_1=0.7. Figure 10 shows the steady-state solution for p_o/p_e= 22,25,30 and 100. The corresponding variation of centre-line pressure and mach number is shown in Figure 11. It can be observed that for p_o/p_e= 25,30 and 100 the flow in the test-section is almost same but significant differences are observed in the diffuser section. For p_o/p_e= 100, the diffuser does very little and in fact most of the flow at the exit is supersonic and accelerates in the divergent part. The separation point of the flow in the diffuser moves upstream as the pressure ratio decreases and at p_o/p_e = 22 reach the later part of the nozzle block. From this study it is clear that the tunnel may not be able to operate below p_o/p_e = 25 with the present diffuser section.

In the last part of this study the effect of the length of the constant-area section (Lc) of the diffuser is investigated. Computations are carried out for A_2/A_1=0.7, p_o/p_e = 22 and for Lc= 8.8, 8.0 and 7.2. Figures 12 and 13 show the steady -state solutions for these three cases. In the cases with Lc= 8.0 and 7.2 the tunnel fails to provide a fully developed flow in the test-section. However the case with Lc = 8.8 seems to result in an acceptable flow. It should be pointed out that the increase in the diffuser length may not always lead to an improvement in the flow quality beyond a certain length the losses due to friction (Fanno effect) may dominate and lead to a loss in the diffuser efficiency.

CONCLUDING REMARKS

A finite element method has been developed and implemented for the computation of unsteady, viscous flow in a supersonic wind tunnel. Computations have been carried out for a model tunnel with a Mach 5 minimum length nozzle. The effect of changing various parameters in the diffuser geometry has been investigated.

REFERENCES

1) S Mittal. Finite element computation of unsteady viscous compressible flows. Computer Methods in Applied Mechanics and Engineering, 157:151-175, 1998.

2) S Mittal. Finite element computation of unsteady viscous transonic flows past stationary airfoils. Computational Mechanics, 21:172-188, 1998.

3) S.T. Polsky and J.L. Cambier. Numerical study of transient flow phenomena in shock tunnels. AIAA Journal, 32(5):971-978, May 1994.

4) C.L. Chen and S.R. Chakravarthy. Numerical investigation of separated nozzle flows. AIAA Journal, 32(5): 9

5) BM Argro, G Emanuel., Computational Analysis of the Transonic flow field of two dimensional minimum length nozzles, J. Fluids Eng. Trans of the ASME, 113;479-488, Sept 1991.

6) TJR Hughes, M Mallet. A new finite element formulation for computational fluid dynamics. IV. A discontinuity-capturing operation for multidimensional advective-diffusive systems. Comp. Methods in App. Mech. Engg., 58: 329-339,1986.

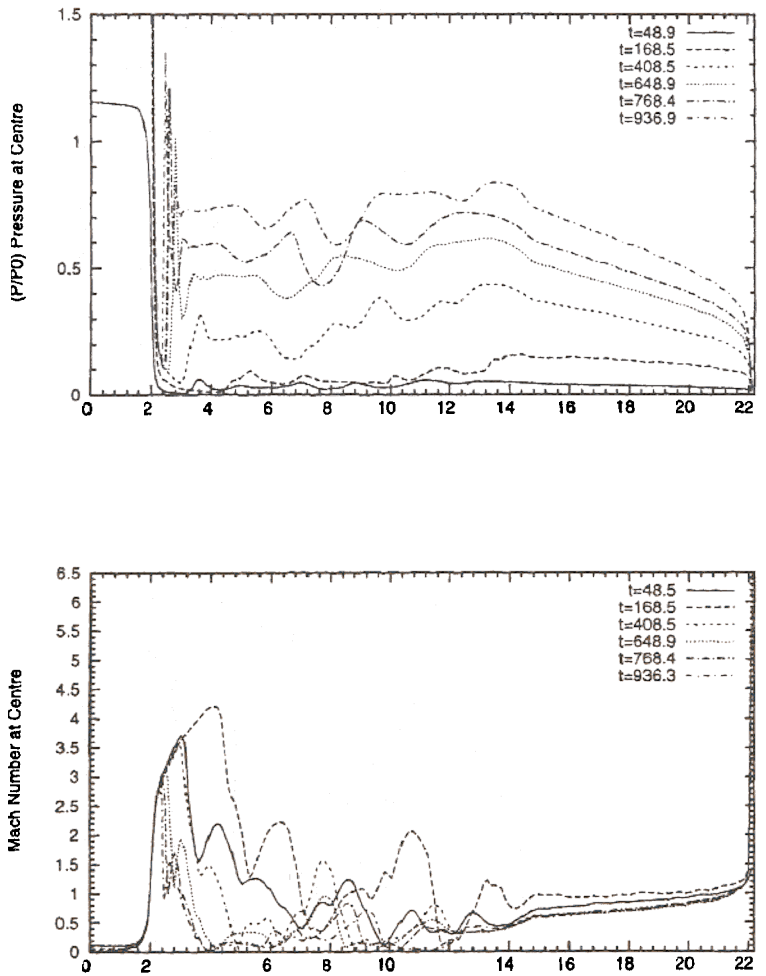

Figure 3. Supersonic flow through a wind-tunnel, $A_2/A_1 = 0.3$, $p_o/p_e = 500$, $L_c = 8$: variation of the pressure and Mach number along the tunnel center-line for various time instants.

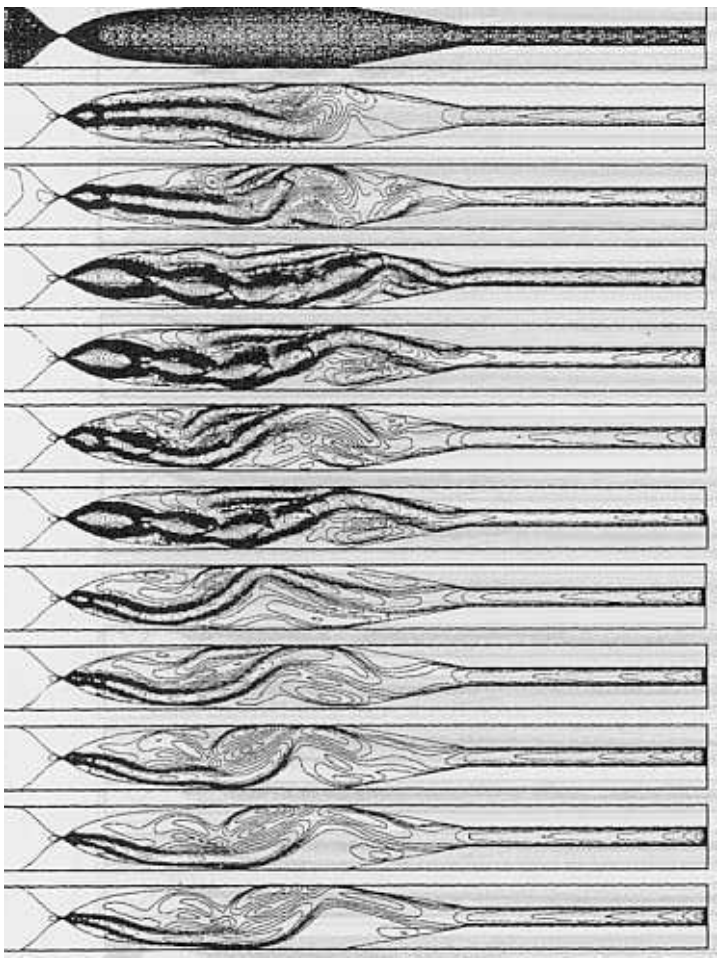

Figure 2. Supersonic flow through a wind-tunnel, $A_2/A_1 = 0.3$, $p_o/p_e = 500$, $L_c = 8$: the finite element mesh and the iso-mach contours for various time instants (from top to bottom) t=22.6, 48.6, 168.6, 288.6, 408.6, 418.6, 528.6, 648.6, 768.6, 888.6, 936.6.

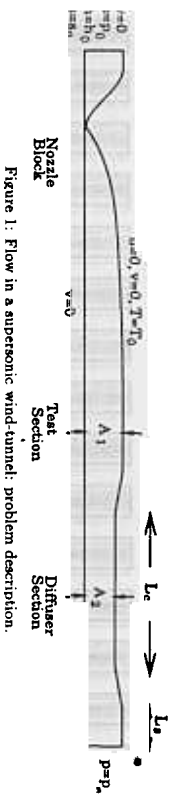

Figure 1: Flow in a supersonic wind-tunnel: problem description.

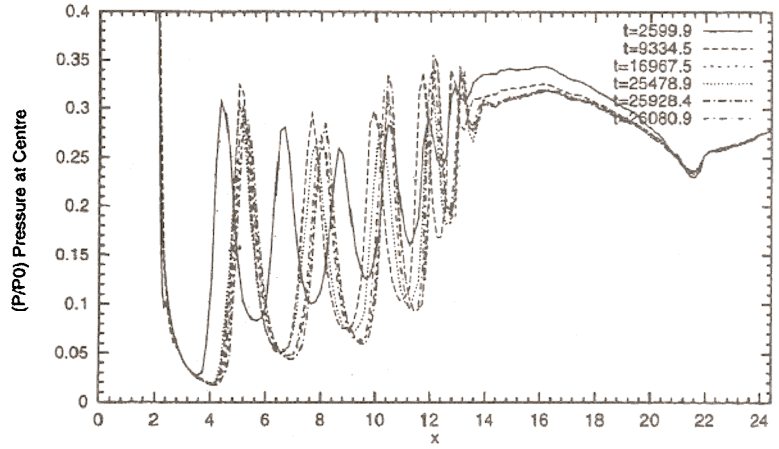

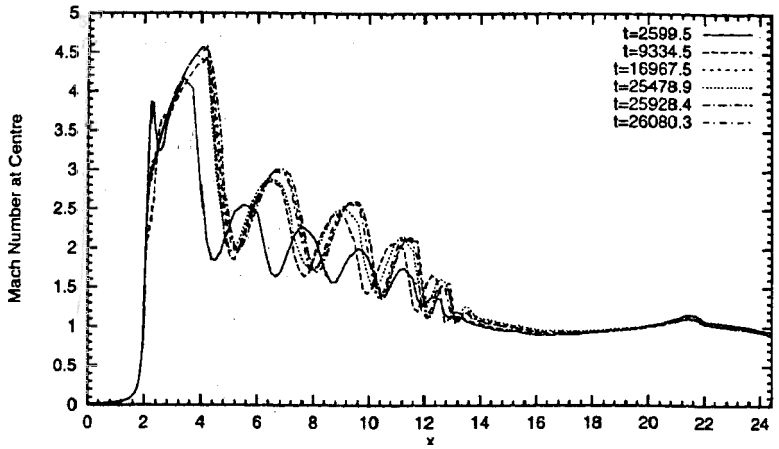

Figure 5. Supersonic flow through a wind-tunnel, $A_2/A_1 = 0.6$, $p_o/p_e = 25$, $L_c = 8$, $L_e =$ variation of the pressure and Mach number along the tunnel center-line for various time instants.

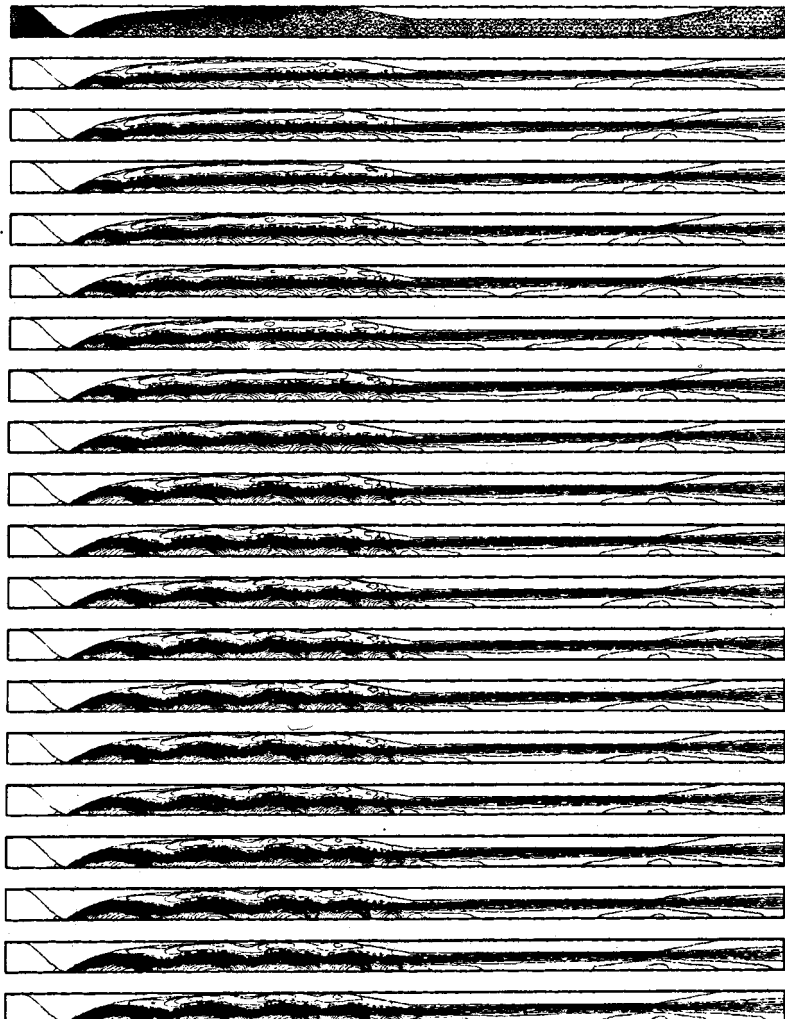

Figure 4. Supersonic flow through a wind-tunnel, $A_2/A_1 = 0.6$, $p_o/p_e = 25$, $L_c = 8$, $L_e = 2$: the finite element mesh and the iso-mach contours for various time instants (from top to bottom) t=142.4, 161.4, 739.4, 951.4 1849.4, 1946.4, 3399.4, 4849.4, 6334.4, 10834, 12319.4, 15319.4, 16819.4, 17117.8, 17417.4, 25478.4, 25778.4

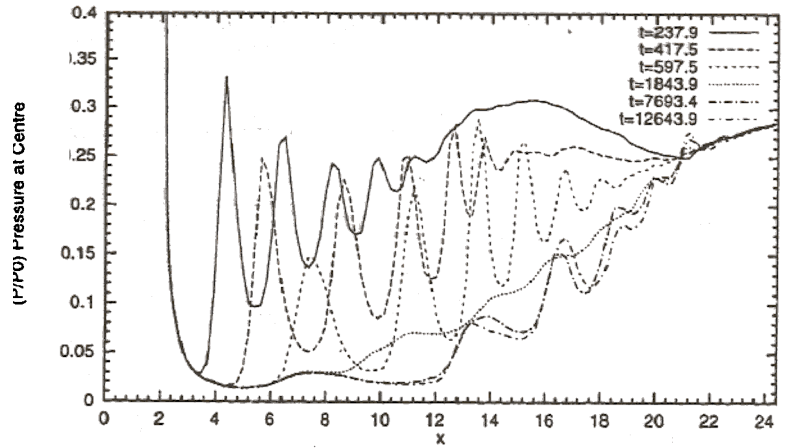

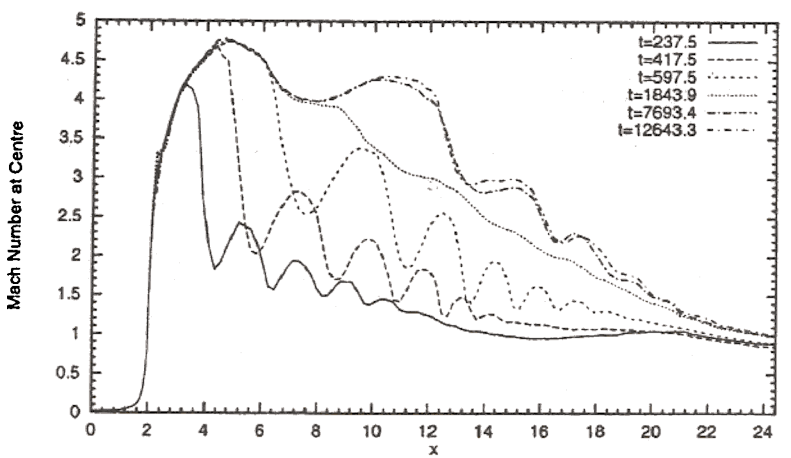

Figure 7. Supersonic flow through a wind-tunnel, $A_2/A_1 = 0.7$, $p_o/p_e = 25$, $L_c = 8$, $L_s = 2$: variation of the pressure and Mach number along the tunnel center-line for various time instants.

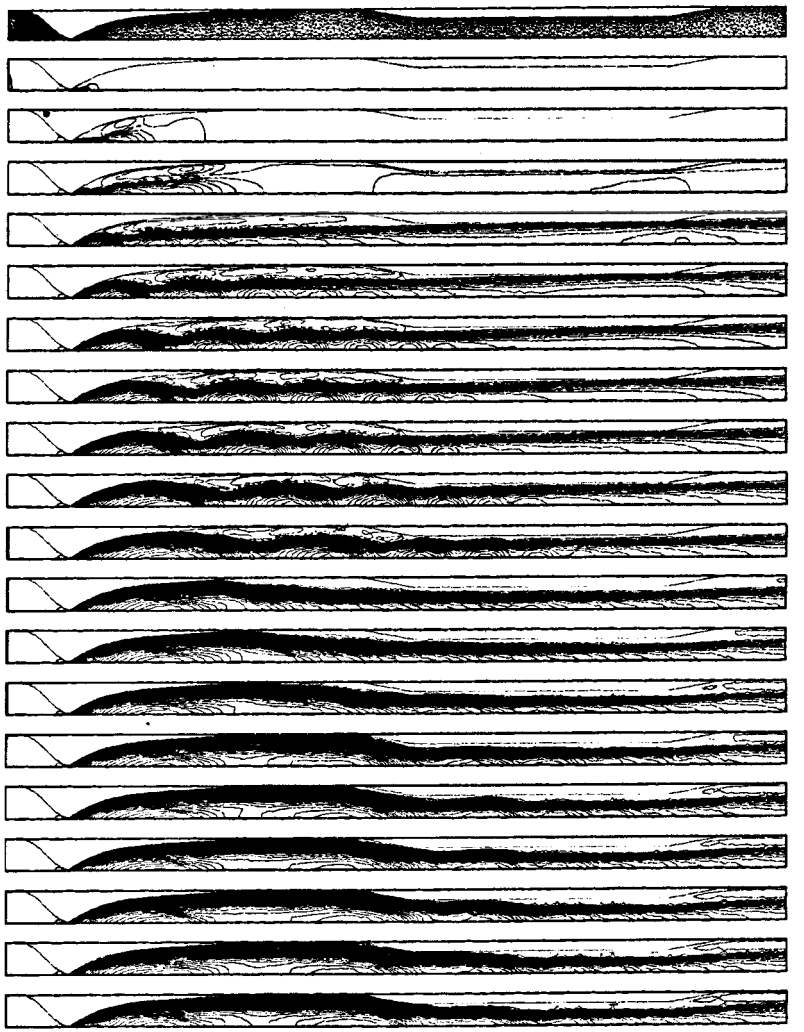

Figure 6. Supersonic flow through a wind-tunnel, $A_2/A_1 = 0.7$, $p_o/p_e = 25$, $L_c = 8$, $L_s = 2$: the finite element mesh and the iso-mach contours for various time instants (from top to bottom) t=31.4, 40.4, 102.4, 192.4, 287.4, 417.4, 552.4, 837.5, 1843.5, 2743.5, 3643.5, 4543.5, 4993.5, 7243.5, 8143.5, 9493.5, 10393.5, 11743.5 and 12643.1.

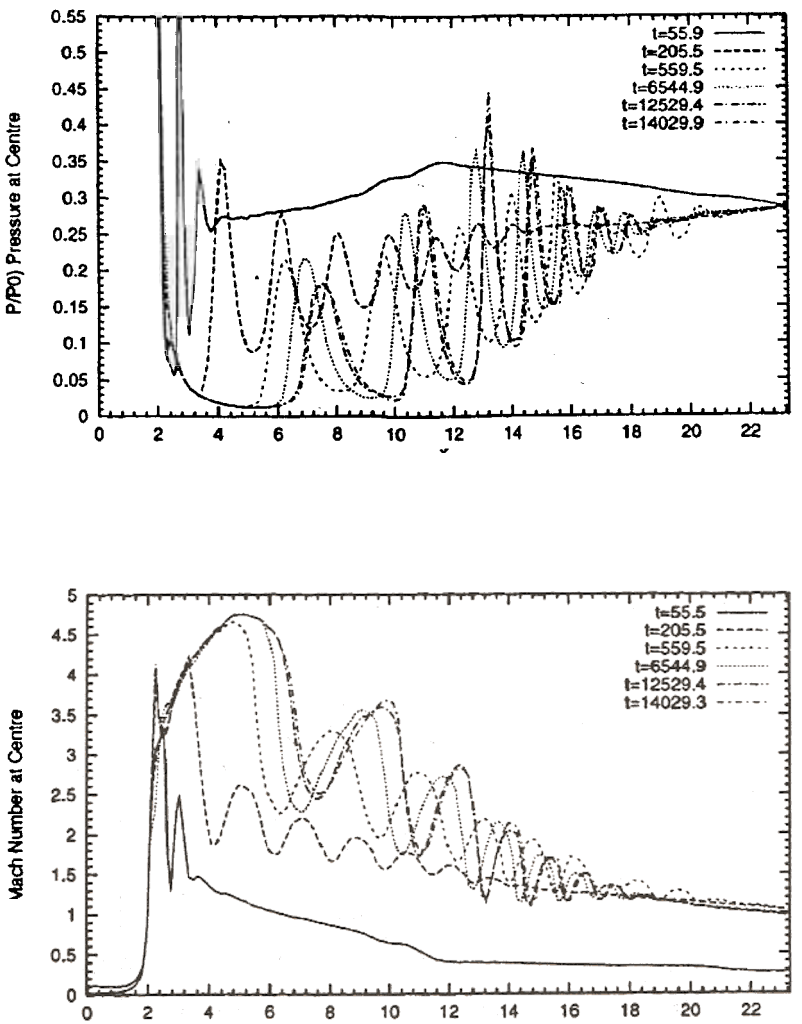

Figure 9. Supersonic flow through a wind-tunnel, $A_2/A_1 = 0.8$, $p_o/p_e = 25$, $L_c = 8$, $L_s = 2$: variation of the pressure and Mach number along the tunnel center-line for various time instants.

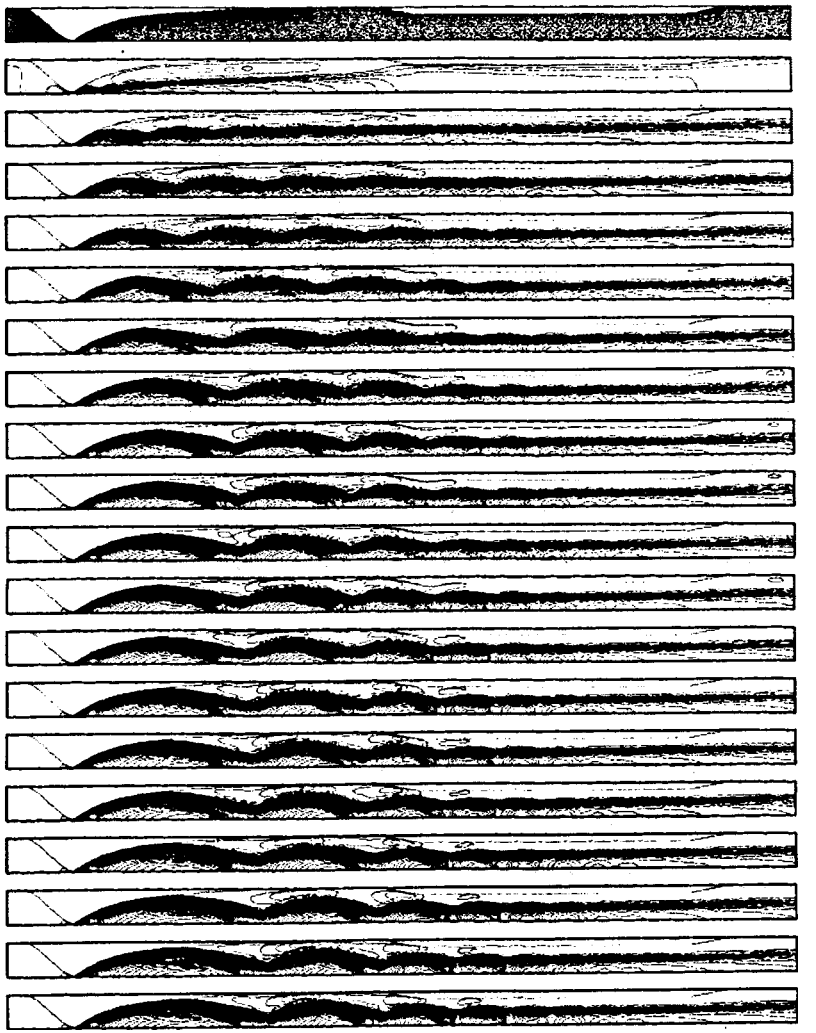

Figure 8 Supersonic flow through a wind-tunnel, $A_2/A_1 = 0.8$, $p_o/p_e = 25$, $L_c = 8$, $L_s = 2$: the finite element mesh and the iso-mach contours for various time instants (from top to bottom) t=55.5, 205.5, 318.5, 355.5, 468.5, 559.5, 1684.5, 2059.5, 3184.5, 3559.5, 4684.5, 5059.5, 6169.5, 7669.5, 8044.5, 9169.5, 10669.5, 12904.5 and 14029.5.

Figure 12. Supersonic flow through a wind-tunnel, $A_2/A_1 = 0.7$, $p_o/p_e = 22$, $L_s = 2$: the iso-mach contours for various values of the length of the constant area section of the diffuser (from top to bottom) $L_c = 8.8$, 8.0 and 7.2

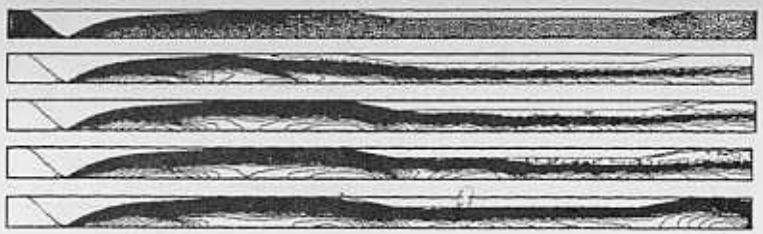

Figure 10. Supersonic flow through a wind-tunnel, $A_2/A_1 = 0.7$, $L_c = 8$, $L_s = 2$: the finite element mesh and the iso-mach contours for various reservoir-to-exit pressure ratios (from top to bottom) $p_o/p_e = 22$, 25, 30 and 100.

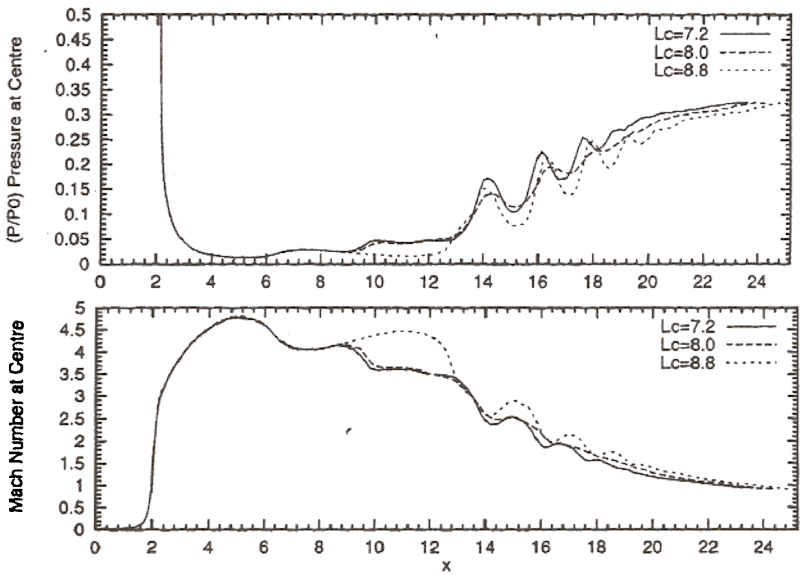

Figure 13. Supersonic flow through a wind-tunnel, $A_2/A_1 = 0.7$, $p_o/p_e = 22$, $L_s = 2$: variation of the pressure and Mach number along the tunnel center-line for various lengths of the constant area section of the diffuser.

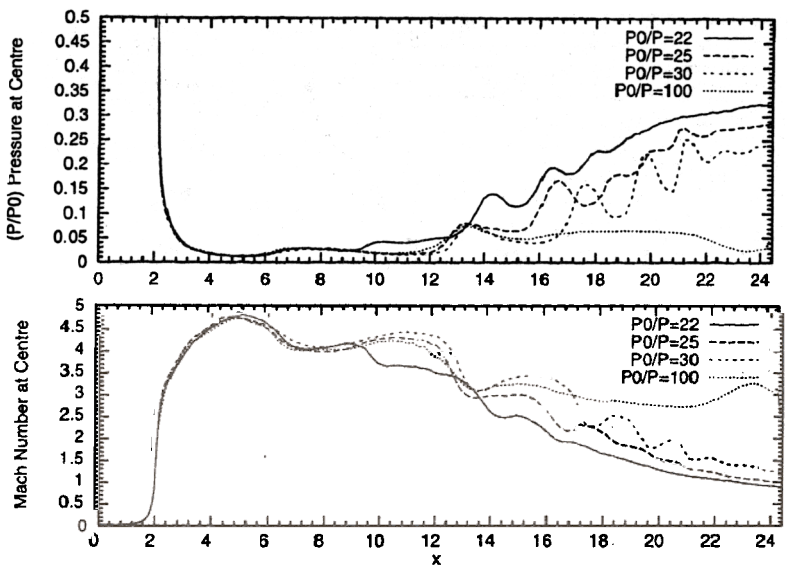

Figure 11. Supersonic flow through a wind-tunnel, $A_2/A_1 = 0.7$, $L_c = 8$, $L_s = 2$: variation of the pressure and Mach number along the tunnel center-line for various reservoir-to-exit pressure ratios.